The State of the Art of Microwave CAD: EM-Based Optimization and Modeling

Qingsha S. Cheng,[1] John W. Bandler,[1] Slawomir Koziel,[2] Mohamed H. Bakr,[1] Stanislav Ogurtsov[2]

[1] Department of Electrical and Computer Engineering, McMaster University, Hamilton, Ontario L8S4K1, Canada
[2] School of Science and Engineering, Reykjavík University, Menntavegur 1, IS-101 Reykjavík, Iceland

Received 19 January 2010; accepted 14 March 2010

ABSTRACT: We briefly review the current state of the art of microwave CAD technologies. We look into the history of design optimization and CAD-oriented modeling of microwave circuits as well as electromagnetics-based optimization techniques. We emphasize certain direct approaches that utilize efficient sensitivity evaluations as well as surrogate-based optimization approaches that greatly enhance electromagnetics-based optimization performance. On the one hand, we review recent adjoint methodologies, on the other we focus on space mapping implementations, including the original, aggressive, implicit, output, tuning, and related developments. We illustrate our presentation with suitable examples and applications. © 2010 Wiley Periodicals, Inc. Int J RF and Microwave CAE 20:475–491, 2010.

Keywords: optimization; adjoint sensitivity; surrogate modeling; space mapping; EM simulator; circuit simulator; tuning

I. INTRODUCTION

The advent of digital computers six decades ago and subsequent technological breakthroughs make possible the simulation-based optimization of high frequency structures. Instead of requiring costly repeated prototyping, actual structures can be accurately modeled using an electromagnetic (EM) simulator and its optimal designable parameter values determined by suitable optimization engines. This approach cuts production costs and reduces product time to market.

EM simulation can be highly accurate but, at the same time, very CPU intensive. This challenges traditional optimization techniques. Researchers tackle the issue on two fronts: (a) the speed-up of EM simulations and, one of the thrusts of this article, the utilization of corresponding EM-based derivative evaluations (adjoint sensitivity analysis), (b) the implementation of suitable surrogate-based approaches such as space mapping.

In Section II of this article, we briefly review some historical benchmarks in microwave circuit design and modeling. In Section III, we review direct optimization approaches with effective sensitivity evaluations, and also surrogate optimization approaches. In Section IV, we discuss an efficient sensitivity analysis technique based on the adjoint concept. We demonstrate the technique with suitable examples. In Section V, we review surrogate optimization, in particular, state-of-the-art space mapping techniques, with applications and examples. We summarize our presentation in Section VI.

Correspondence to: Q. S. Cheng; e-mail: chengq@mcmaster.ca
DOI 10.1002/mmce.20454
Published online 26 July 2010 in Wiley Online Library (wileyonlinelibrary.com).

II. HISTORICAL REVIEW

A. Optimization Theory: Preparation

In 1967 Temes and Calahan [1] presented an extensive review of general-purpose optimization algorithms, many of which are still useful to today's computer-aided design. Theirs was the first comprehensive review of its kind in the circuits and systems area. In the microwave arena, Bandler [2] discussed one-dimensional methods, such as Fibonacci Search, Golden Section search, interpolation methods, etc. In his review of multidimensional direct search techniques, Bandler [2] described one-at-a-time search, Pattern Search, the Rotating Coordinates method, Powell's Method, and Simplex methods. He reviewed multidimensional gradient strategies, such as steepest descent, Newton-Raphson, Fletcher-Powell, least squares, least *p*th, etc.

B. Optimization and Modeling in the Microwave Arena

Bandler [2, 3] systematically treated the formulation of error functions w.r.t. design specifications. He explored generalized least *p*th and minimax objectives, as well as

adjoint circuit sensitivity analysis techniques suitable for microwave circuit simulation and design. The size and complexity of microwave devices continued to increase, especially after the emergence of MMICs [4] in the 1970s. Addressing this issue, Bandler et al. [5] demonstrated the automated minimax optimization of a 12 GHz multiplexer with 16 channels and 240 nonlinear design variables.

Physics-based models provide engineers the flexibility of performing designs based on physical parameters and to foresee the circuit characteristics before fabrication. The year 1992 saw advances [6] in device modeling, parameter extraction, nonlinear simulation, nominal design, statistical modeling, and yield optimization in the context of such physics-oriented microwave circuit optimization. Topics included analytical large-signal physical models of MESFETs and nonlinear circuit analysis with physics-based models integrated into the harmonic balance equations.

C. Microwave CAD Software

In 1988, Bandler and Chen [7] emphasized optimization-oriented approaches that deal with process imprecision, manufacturing tolerances, model uncertainties, measurement errors, and so on, approaches well-suited to yield-driven design and cost reduction for integrated circuits. They reviewed realistic representations for nominal (single) circuit optimization, statistical circuit design (design centering), and multicircuit modeling, as well as gradient-based optimization methods. Their article was timely in that Optimization Systems Associates (OSA) was then integrating relevant software into SuperCOMPACT. Bandler and Salama addressed the topic of circuit tuning for postproduction alignment in an earlier article [8].

Les Besser introduced COMPACT (Computer Optimization of Microwave Passive and Active CircuiTs) in 1973. Its successor, SuperCOMPACT, became an industry standard [9]. EEsof launched TOUCHSTONE in 1983. TOUCHSTONE evolved into Libra after the addition of harmonic balance simulation through Microwave Harmonica [9].

Effective multidimensional quadratic functions have been suggested to simultaneously approximate responses and gradients. Relevant theoretical developments were incorporated into OSA90/hope [10] and HarPE [10]. OSA90/hope's novel Datapipe structure constituted the first microwave CAD product of its kind. This open architecture feature enabled device and circuit designers to solve relevant linear/nonlinear/statistical modeling, simulation, and optimization problems with both circuit and physical parameters.

Techniques for design centering, tolerance assignment, worst-case, and statistical design, and postproduction tuning evolved during the 1970's [11]. In the late 1980's OSA introduced yield-driven design into SuperCOMPACT. EEsof followed suit with yield-driven design options. The 1980's also saw advances and robust implementation of gradient-based algorithms for minimax, l_1, and l_2 optimization [7].

D. Optimization Using EM Simulators

During the 1980's, Ansoft Corporation, Hewlett-Packard, and Sonnet Software embarked on the development of simulators that solved Maxwell's equations for complex geometries. These EM simulators or solvers were originally used to obtain accurate simulations or validations of complex microwave structures.

The idea of employing EM solvers for direct optimization attracted microwave engineers. However, EM solvers are CPU-intensive and, as originally construed, also suffered from nondifferentiable response evaluation and nonparameterized design variables that were discrete in the parameter space. These characteristics are unfriendly to gradient optimization algorithms. To alleviate this, Bandler et al. proposed the utilization of databases [10], Datapipe [10], multidimensional interpolation [10, 12], Geometry Capture [10, 13] for parameterization, and the pragmatic idea of the ''simulation grid.'' Formal EM optimization of microwave structures has been reported since 1994 [14–17]. OSA90/hope [10] provided an interface to external simulators, circuit based or EM based.

Highlights from 2004 [18] include the article by De Zutter et al. [19], which provides an overview of the general EM circuit co-optimization approach based on an EM database. Rautio describes [20] a method for joining small subsections so that the large subsections so formed can follow the arbitrarily curving edges of a complicated circuit while including the high edge current. Using such conformal subsections, nonManhattan geometries, such as circular spiral inductors, can be effectively analyzed. Mattes and Mosig [21] present a new adaptive sampling to accelerate frequency-domain calculations using genetic algorithms and rational functions to approximate the frequency response. Hussein and El-Ghazaly [22] deal with global modeling of microwave devices where they consider Maxwell's equations in conjunction with a hydrodynamic model. They solve these equations through a real-coded genetic algorithm and an appropriate objective function.

E. Adjoint Sensitivities for EM Models

The adjoint sensitivity approach dates back to the 1960s work of Director and Rohrer [23, 24]. Bandler et al. also addressed adjoint circuit sensitivities, e.g., [25–28], in the context of microwave design.

Interest in EM-based adjoint calculations was revived after the work [29] was published. Since 2000, a number of interesting publications addressed the application of the so-called adjoint variable method (AVM) to different numerical EM solvers. These include the time-domain transmission-line modeling (TLM) method [30–34], the finite-difference time-domain (FDTD) method [35–38], the finite-element method (FEM) [39, 40], the method of moments (MoM) [41–43], the frequency domain TLM [44, 45], the mode-matching method (MM) [46, 47], and the beam propagation method (BPM) [29, 48]. These approaches can be classified as either time-domain adjoint variable methods or frequency-domain adjoint variable methods.

F. Surrogate Optimization of EM Models

The successful interconnection of EM solvers with powerful optimization techniques partially solved the EM-based design bottleneck, as EM simulation remained CPU-intensive. Since the 1990s, EM modeling and optimization have been explored through novel technologies that include response surface modeling [12], model-reduction techniques [49], artificial neural networks [50], and surrogate-base optimization (SBO) [51].

The so-called space mapping approach, recognized as an SBO method, was introduced by Bandler et al. [52]. In [53, 54], the authors review various concepts of space mapping and place them contextually into the history of design optimization and modeling of microwave circuits. They formulate a generic space mapping optimization algorithm, explain it in a step-by-step fashion, and demonstrate its robustness through the fast design of an interdigital filter. Selected topics of space mapping are also discussed, including implicit space mapping, gradient-based space mapping, the optimal choice of a surrogate model, and—recently—tuning space mapping, as well as applications for modeling of microwave structures. They also discuss a state-of-the-art software package for automated space mapping optimization involving electromagnetic and circuit simulators.

In [55], the authors discuss a tuning space mapping procedure and its implementation that encompasses the port tuning method. Circuit theory based tuning elements are inserted into EM simulator via the tuning port to form a surrogate.

III. HIGH PERFORMANCE EM-BASED OPTIMIZATION

A. The Optimization Problem

The design optimization problem to be solved is given by

$$\boldsymbol{x}^* = \arg\min_{\boldsymbol{x}} U(\boldsymbol{R}_f(\boldsymbol{x})) \tag{1}$$

where $\boldsymbol{R}_f \in \Re^{m\times 1}$ is a vector of m responses of the EM model, e.g., $|S_{11}|$ at m selected frequency points, $\boldsymbol{x}$ is the vector of n design parameters and U is a suitable objective function. For example, U could be a minimax objective function with upper and lower specifications. Here, $\boldsymbol{x}^*$ is the optimal solution to be determined. It is assumed to be unique.

A typical gradient based optimization algorithm (optimizer) requires function values and derivatives or response sensitivities. See Figure 1. Sensitivity information enables the designer to determine the parameters of most influence on the response and predict how the response would change by changing these parameters. Classically, finite difference approximations are used to estimate the required derivatives.

Typical gradient optimization algorithms may require hundreds of expensive iterations. This burden motivates research into alternative approaches such as the adjoint sensitivity approach. We focus here on the time-domain AVM in Section IV.

B. Surrogate-Based Approach

A fundamental issue is the high cost of EM simulation. Simulation-based tasks, such as parametric optimization or statistical design centering, are typically infeasible when performed directly using CPU-intensive EM models. An effective way to overcome this problem is by using suitable cheap surrogates.

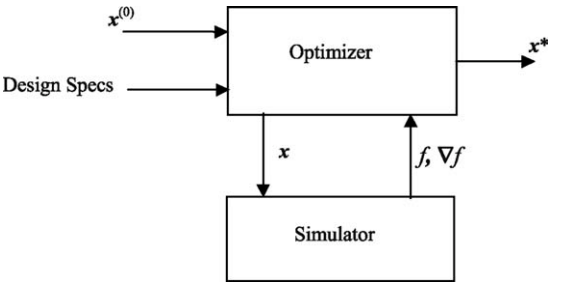

Figure 1 A gradient-based optimizer utilizes both the response and its gradient.

Surrogate models can be categorized into functional and physical [56]. Functional surrogates are created through data pairs (designs and corresponding responses) obtained by sampling the design space of a given microwave structure. Popular methods include polynomial approximation, radial basis function interpolation [57], kriging [58], support vector regression [59], and neural networks [60]. For good accuracy, these techniques require many training points, and are therefore suitable in creating multiple-use library models. Physical surrogates, on the other hand, are based on low-fidelity (or coarse) models that embed physical phenomena already encoded in the original, high-fidelity model. In microwave engineering, such coarse models include equivalent circuits and coarse-grid EM models. Typically, physical surrogates ensure good accuracy even though a limited number of training points is used to set them up, which makes them suitable for tasks such as design optimization or statistical analysis.

Both functional and physical models can be exploited in so-called surrogate-based optimization [51]. The generic SBO optimization algorithm can be formulated as follows:

$$\boldsymbol{x}^{(i+1)} = \arg\min_{\boldsymbol{x}} U(\boldsymbol{R}_s^{(i)}(\boldsymbol{x})) \tag{2}$$

where $\boldsymbol{x}^{(i)}$, $i = 0, 1, \ldots$, is the sequence of approximate solutions to the original design problem $\boldsymbol{x}^* = \text{argmin}\{\boldsymbol{x}: U(\boldsymbol{R}_f(\boldsymbol{x}))\}$. Here, $\boldsymbol{x}^{(0)}$ is the initial design. If $\boldsymbol{R}_s^{(i)}$ is a computationally cheap and sufficiently reliable representation of the fine model, particularly in the neighborhood of the current design $\boldsymbol{x}^{(i)}$, the algorithm (2) is likely to produce a sequence of designs that quickly approach $\boldsymbol{x}^*$.

Usually, $\boldsymbol{R}_f$ is only evaluated once per iteration (at every new design $\boldsymbol{x}^{(i+1)}$) for verification purposes and to obtain the data necessary to update the surrogate model. If the surrogate model is computationally cheap, its optimization cost (cf. (1)) does not substantially influence the total optimization cost. The number of evaluations of $\boldsymbol{R}_f$ for a well-performing surrogate-based algorithm is substantially smaller than for any direct optimization method (e.g., gradient-based one) [61].

If the surrogate model satisfies zero- and first-order consistency conditions with the fine model, i.e., $\boldsymbol{R}_s^{(i)}(\boldsymbol{x}^{(i)}) =$

$\boldsymbol{R}_f(\boldsymbol{x}^{(i)})$ and $(\partial \boldsymbol{R}_s^{(i)}/\partial \boldsymbol{x})(\boldsymbol{x}^{(i)}) = (\partial \boldsymbol{R}_f/\partial \boldsymbol{x})(\boldsymbol{x}^{(i)})$, and the algorithm (2) is enhanced by the trust region method [61, 62], then it is provably convergent to a local optimum of the fine model [63]. Convergence can also be guaranteed if the algorithm (2) is enhanced by properly selected local search methods [64]. Some of the available space mapping approaches are based on ensuring first-order consistency, including Generalized Implicit Space Mapping [61], Manifold Mapping [65], and corrected space mapping [66].

Other approaches, popular in aerospace and structural engineering, include approximation and model management [64], surrogate management framework [67], SBO techniques based on surface response approximation and kriging [68], as well as a combination of surrogate modeling with evolutionary optimization [69].

Space mapping is probably the most popular SBO approach used in microwave engineering. In Section V, we review and discuss the original, aggressive, implicit, output, and tuning space mapping.

IV. ADJOINT SENSITIVITY ANALYSIS

A. Introduction

The basic concept behind all adjoint sensitivity analysis approaches is to construct another circuit called the adjoint circuit. This circuit supplies the adjoint response. The simulation time of this circuit should be comparable to that of the original simulation. Using the original circuit response $\boldsymbol{R}(\boldsymbol{x})$ and the adjoint circuit response $\tilde{\boldsymbol{R}}(\boldsymbol{x})$, the gradient is estimated. It follows that the cost of one gradient estimation is reduced to only one extra simulation regardless of n. This makes this approach particularly attractive for problems where n is large or when the computational cost of one simulation is high.

In [29], the authors employ both the FDTD and finite-element time-domain (FETD) approaches together. They estimate the sensitivities of a given objective function using only one extra adjoint simulation. Because this approach utilizes a combination of techniques, it is less attractive.

The target of EM optimization is to determine an optimal set of values $\boldsymbol{x}^*$ of the designable parameters as the solution of the optimization problem:

$$\boldsymbol{x}^* = \arg\min_{\boldsymbol{x}} F(\boldsymbol{x}, \boldsymbol{R}(\boldsymbol{x})) \tag{3}$$

where F is the objective function, and $\boldsymbol{R}$ is a vector of responses that are calculated using the electromagnetic solution $\boldsymbol{E}$. Notice that the objective function has been extended from (1) to include both explicit and implicit dependence on $\boldsymbol{x}$ through $\boldsymbol{R}$. If the explicit dependence is zero, the F of (3) becomes equivalent to the U of (1).

B. Time-Domain Adjoint Sensitivities [30]–[36]

For time-domain simulators, the objective function includes an integral of time-domain values, and it can be put in the form

$$F = \int_0^{T_s} \psi(\boldsymbol{x}, \boldsymbol{R}) dt \tag{4}$$

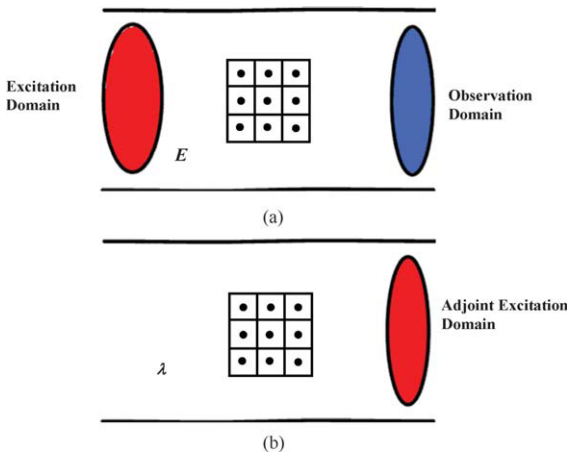

Figure 2 The AVM approach: (a) the original simulation and (b) the adjoint simulation where the observation domain becomes the excitation domain. The field is stored at the locations indicated by the dots in both simulations. [Color figure can be viewed in the online issue, which is available at wileyonlinelibrary.com.]

where T_s is the simulation time. The derivative of F with respect to the ith parameter is given by

$$\frac{\partial F}{\partial x_i} = \int_0^{T_s} \frac{\partial^e \psi}{\partial x_i} dt + \int_0^{T_s} \frac{\partial \psi}{\partial \boldsymbol{R}^T} \frac{\partial \boldsymbol{R}}{\partial x_i} dt, \quad i = 1, 2, \ldots, n \tag{5}$$

Note that the first integral in (5) is the explicit dependence of the objective function. The second integral contains the dependency of the objective function on the design parameters through the responses.

For both TLM and FDTD, the actual simulation is given by

$$\boldsymbol{M}\ddot{\boldsymbol{E}} + \boldsymbol{N}\dot{\boldsymbol{E}} + \boldsymbol{K}\boldsymbol{E} + \int_0^t \boldsymbol{G}(t-\tau)\boldsymbol{E}(\tau) d\tau = \boldsymbol{Q} \tag{6}$$

The matrices $\boldsymbol{M}$, $\boldsymbol{N}$, and $\boldsymbol{K}$ are functions of the space discretization, the material properties, and the design parameters. Vector $\boldsymbol{E}$ represents the field solution in FDTD or the vector of incident impulses in the TLM method. The matrix $\boldsymbol{G}$ is the time-domain Green's function of the boundary and is assumed parameter independent. The vector $\boldsymbol{Q}$ is the excitation term and is assumed to vary according to a known time profile. The domain where $\boldsymbol{Q}$ is nonzero is called the excitation domain. The matrices $\boldsymbol{M}$, $\boldsymbol{N}$ and $\boldsymbol{K}$ are time-independent. We assume that (6) is solved with zero initial field conditions $\boldsymbol{E}(0) = \boldsymbol{0}$ and $\dot{\boldsymbol{E}}(0) = \boldsymbol{0}$. The objective function F of (4) is calculated using the time-domain field $\boldsymbol{E}$. The domain in which (4) is calculated is called the observation domain. Figure 2a illustrates the excitation and observation domains for a 2D problem.

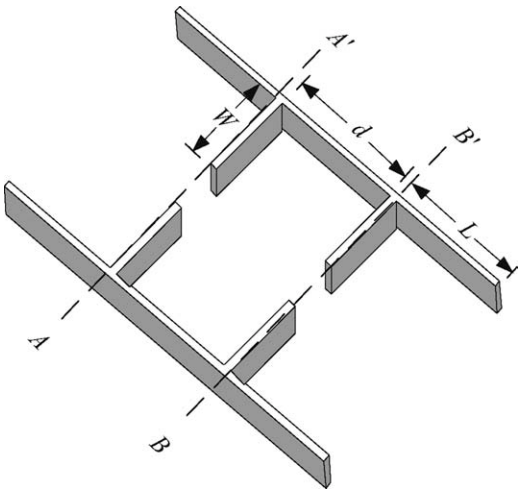

Figure 3 The single-resonator filter [70].

The AVM utilizes an adjoint system of the form:

$$\boldsymbol{M}^T\ddot{\boldsymbol{\lambda}} - \boldsymbol{N}^T\dot{\boldsymbol{\lambda}} + \boldsymbol{K}^T\boldsymbol{\lambda} + \int_0^{T_s} \boldsymbol{G}^T(\tau - t)\boldsymbol{\lambda}(\tau)d\tau = \frac{\partial \psi}{\partial \boldsymbol{E}},$$
$$\boldsymbol{\lambda}(T_s) = \boldsymbol{0} \quad \text{and} \quad \dot{\boldsymbol{\lambda}}(T_s) = \boldsymbol{0} \quad (7)$$

The adjoint system (7) supplies the vector of adjoint fields $\boldsymbol{\lambda}$ at all time steps. Note that (7) defines a backward adjoint simulation. Starting at a time $t = T_s$, the adjoint simulation runs backward in time to get the values of the vector $\boldsymbol{\lambda}$ at all time steps. Note also that the adjoint excitation $\partial\psi/\partial\boldsymbol{R}$ is determined through the original simulation and is nonzero only within the observation domain (Fig. 2b).

Once the $\boldsymbol{E}$ vectors are determined using the original simulation (6) and the adjoint response $\boldsymbol{\lambda}$ is determined using (7) for all time steps, the sensitivities of F with respect to all parameters are determined from

$$\frac{\partial F}{\partial x_i} = \int_0^{T_s} \boldsymbol{\lambda}^T \left[\frac{\Delta \boldsymbol{Q}}{\Delta x_i} - \frac{\Delta \boldsymbol{M}}{\Delta x_i}\ddot{\boldsymbol{E}} - \frac{\Delta \boldsymbol{N}}{\Delta x_i}\dot{\boldsymbol{E}} - \frac{\Delta \boldsymbol{K}}{\Delta x_i}\boldsymbol{E}\right] dt \quad (8)$$

Note that the perturbation of the system matrices or excitation are assumed known for a given perturbation of any parameter. It follows that by using original simulation (6) and adjoint simulation (7), we can estimate the sensitivities of the objective function with respect to all parameters regardless of their number.

The expression (8) requires storing of both the original field $\boldsymbol{E}$ and the adjoint field $\boldsymbol{\lambda}$ where the system matrices undergo a parameter change. For a change in the dielectric property of an object, both fields have to be stored inside the objects for all the time steps, as shown in Figure 2.

To illustrate the AVM approach, we consider the single resonator filter shown in Figure 3. This filter was simulated using 2D TLM with a modal Johns matrix boundary [30]. This boundary implements the integral in (6) but for only one mode, resulting in a reduction in computational cost. The waveguide length and width are 16.0 cm and 6.0 cm, respectively. A TLM cell of dimension 1.0 mm is utilized. Our objective function is of the form

$$\boldsymbol{F}(\boldsymbol{x}, \boldsymbol{V}) = \Delta t \sum_{k=1}^{N_t} \sum_{i=1}^{Nx} V_{3,k}^2(i, N_z) \quad (9)$$

where $V_{3,k}$ is the value of the incident field at the 3rd link at the kth time step. The objective function (9) measures the power delivered to the output port. The waveguide is excited with a Gaussian-modulated sinusoidal signal centered at ω_o=3.5 GHz.

The sensitivities of (9) are estimated using both the AVM approach and central differences. Figure 4 compares both approaches for a sweep of the parameters d and W, respectively.

C. S-Parameter Calculations

S-parameters are usually calculated in time-domain solvers by applying the Fourier transform to time-domain data stored at ports of interest. For example, the output spectrum at the pth port due to an excitation at the qth port of a multiport circuit is given by

$$\tilde{E}_{pq}(f_o) = \int_0^{T_s} \left\{ \iint_{pth\ port} E(t, \boldsymbol{r})\, E_p(\boldsymbol{r}) ds \right\} \exp(-2\pi\sqrt{-1} f_o\, t) dt \quad (10)$$

In (10), the field at the pth port is first correlated with the modal distribution of the desired mode at the pth port $E_p(\boldsymbol{r})$. The Fourier transform is then applied to the surface integral. The complex objective function (10) can be divided into two real objective functions similar to (4). This

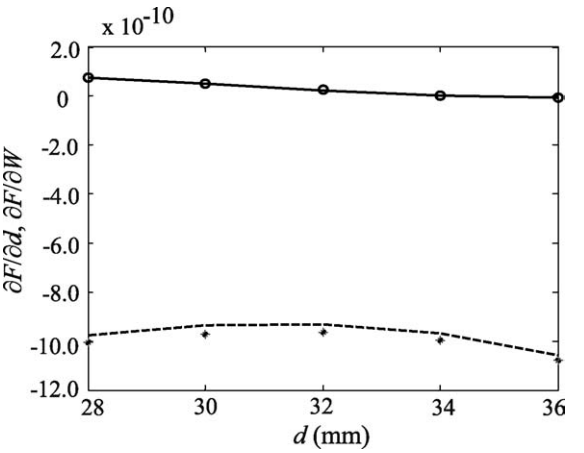

Figure 4 Objective function sensitivities for the single-resonator filter example at $W = 13\Delta l$ with $\Delta l = 1.0$ mm for different values of d; $\partial F/\partial d$ obtained using AVM (o), $\partial F/\partial d$ obtained using central differences (—), $\partial F/\partial W$ obtained using AVM (*), and $\partial F/\partial W$ obtained using central differences (--).

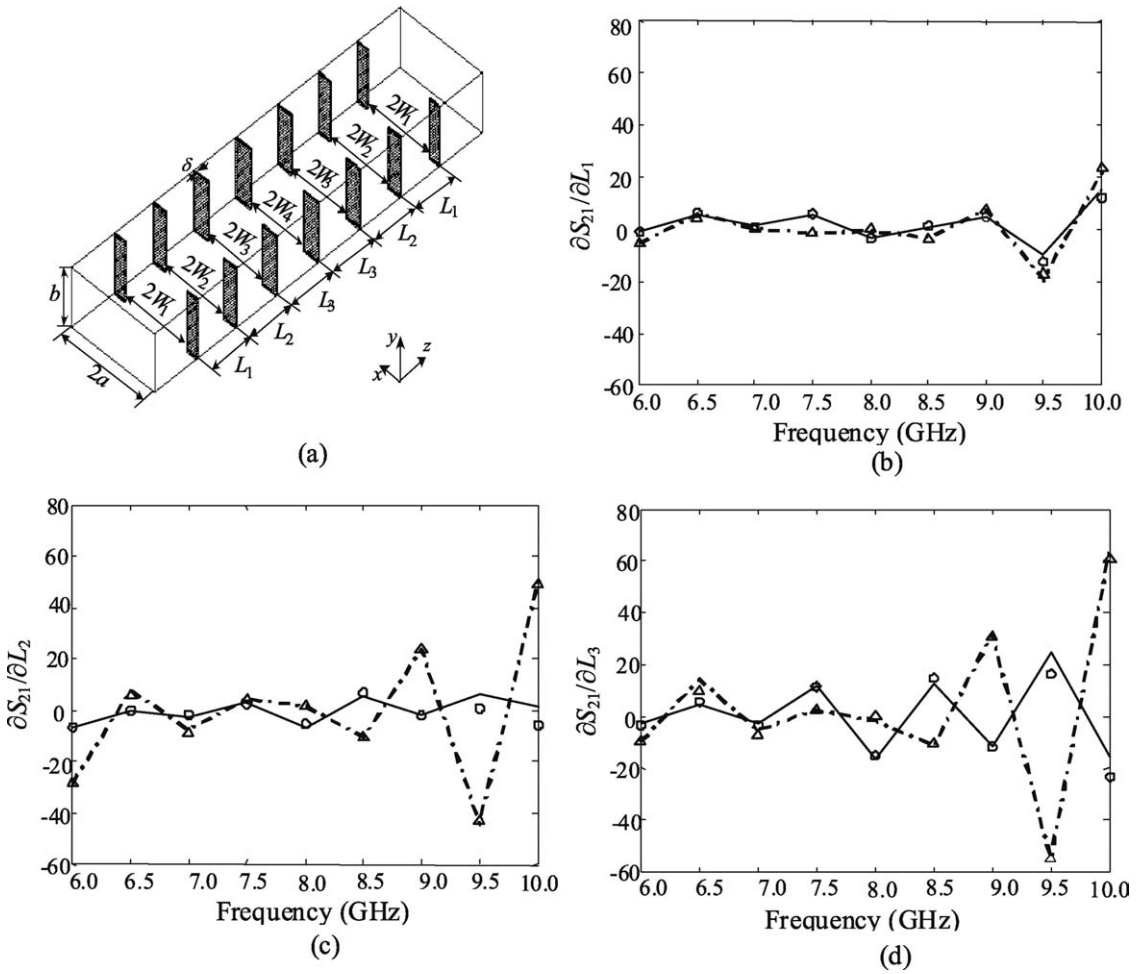

Figure 5 (a) The seven section H-plane filter and, for a sweep of frequencies, the sensitivities of S_{21} relative to (a) spacing L_1, (b) spacing L_2, and (c) spacing L_3. The imaginary part's sensitivities obtained through AVM (—); the imaginary part's sensitivities obtained using central differences (o); the real part's sensitivities obtained through AVM (--); and the real part's sensitivities obtained using central differences (Δ).

implies that two sinusoidal adjoint excitations are required to obtain the sensitivities of the real and imaginary parts with respect to all parameters. In [32], it was shown that the derivatives of the real and imaginary part of the spectrum (10) can be obtained using only a single sinusoidal excitation with frequency f_o. It was also shown that wideband S-parameter sensitivities can be estimated using a wideband adjoint excitation. The approach reported in [32] requires N_p extra adjoint simulations to estimate the sensitivities of all the S-parameters with respect to all parameters regardless of their number and regardless of the number of frequency points. This work was the first to show an algorithm for obtaining wideband adjoint sensitivities of the S-parameters using a time-domain solver.

Figure 5 shows a seven section H-plane filter simulated using the TLM method [32]. The cell size is 0.6223 mm. The waveguide length and width are $301\Delta z$ and $56\Delta x$, respectively. The vector of designable parameters is $\boldsymbol{x} = [L_1\ L_2\ L_3\ W_1\ W_2\ W_3\ W_4]^T$. The waveguide is excited with a Gaussian-modulated sinusoidal waveform centered at frequency $\omega_o = 8.0$ GHz. The sensitivities of S_{21} are estimated using the AVM approach with central differences for nine frequencies in the range 6.0 GHz to 10.0 GHz. These sensitivities are evaluated for the set of parameter values $[L_1\ L_2\ L_3\ W_1\ W_2\ W_3\ W_4\ ]^T = [22\Delta z\ 26\Delta z\ 27\Delta z\ 21\Delta x\ 19\Delta x\ 18\Delta x\ 18\Delta x]^T$. We show only the sensitivities with respect to the lengths. Note that the central difference approximation requires 15 TLM simulations while the AVM approach requires only 2 simulations.

D. The Self-Adjoint Approach

The self adjoint concept was first presented [33] for estimating the S-parameters. This concept states that for some objective functions there is no need for an adjoint simulation (7). The vector of adjoint fields $\boldsymbol{\lambda}$ is deduced from the vector of original fields $\boldsymbol{E}$ for all time steps. This is the case when the excitation domain and the observation domain are the same and when the original excitation $\boldsymbol{Q}$ has a similar spatial and temporal profile to the adjoint excitation $\partial\psi/\partial\boldsymbol{R}$. This applies to the S-parameters because

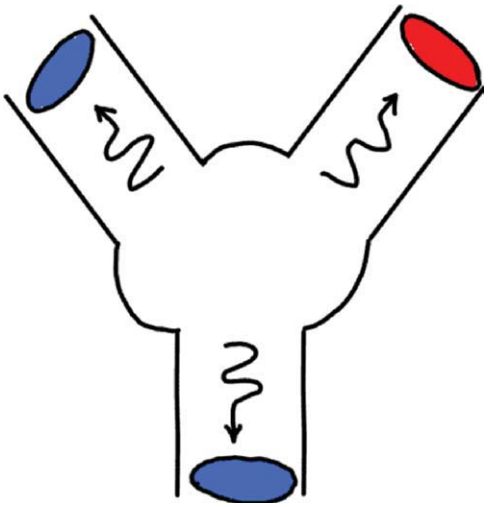

Figure 6 The calculations of the *S*-parameters for a multiport circuit. One port is excited and the fields at all other ports are observed. For calculating all *S*-parameters the ports are excited one at a time. [Color figure can be viewed in the online issue, which is available at wileyonlinelibrary.com.]

ports are excited with the modal distribution one at a time and the modal field is observed at all other ports (Fig. 6). In [33], it was shown that for TLM, the adjoint impulses utilized in calculating the *S*-parameter sensitivities are deducible from the original impulses through the mapping

$$\boldsymbol{\lambda}(\tau) = -\frac{1}{\mu}\boldsymbol{A}\boldsymbol{R}(T_s - \tau) \tag{11}$$

where μ and $\boldsymbol{A}$ are a known scaling factor and matrix, respectively. It follows that adjoint simulations can be predicted from the original simulation (6) through scaling and time shifting.

To illustrate the self adjoint approach, we consider a loaded Tee junction (Fig. 7) simulated using TLM [33]. The designable parameters are the dimensions $\boldsymbol{x} = [d\ W]^T$. The waveguide is excited with a Gaussian-modulated sinusoidal signal centered at f_o=7.5 GHz. The sensitivities are estimated at $[d\ W]^T = [4\Delta z\ 4\Delta x]^T$. Figure 8 shows a good match between the self adjoint sensitivities and those obtained using central differences.

The self adjoint approach was also developed for the FDTD approach [36] and later extended to the general nonhomogenous case of TLM [34].

The main difficulty in all time-domain AVM techniques is the large storage of field components. Field components have to be stored for all time steps at possibly big subdomains of the computational domain. Several improvements were suggested recently to reduce the memory storage of the technique. An algorithm was presented in [37] that limits the required storage needed to estimate the sensitivities. It was shown that the field can be undersampled without sacrificing the accuracy of the estimated sensitivities. Figure 9 shows how the field is sampled within a dielectric object. The sampling rate can go down to a quarter wavelength without sacrificing accuracy. A typical result for a 2D FDTD simulation is shown in Figure 10. It shows that for sampling rates above $20\Delta h$, the accuracy of the sensitivities does not deteriorate.

Another approach to further reduce the required storage [38] exploits the fact that the *S*-parameters are usually calculated for a small discrete number of frequencies. It follows that we can estimate the spectral sensitivities using the spectral components of the field rather than the time-domain field itself. For example, in Figure 2 we may store the spectral components of the field at the dots rather than storing the complete time-domain profile. A saving of $N_T/2N_f$ is possible where N_T is the number of time-domain steps and N_f is the number of frequency points.

V. SPACE MAPPING

A. The Space Mapping Concept

Space mapping technology [52–55] addresses the issue of reducing unnecessary, time-consuming full-wave EM simulations of microwave structures in device modeling and design optimization. The approach involves a calibration of a physically-based ''coarse'' surrogate by a ''fine'' model. This simple CAD methodology embodies the learning process of a designer. It makes effective use of a suitable fast surrogate to sparingly manipulate the iterations of the fine model.

We denote the coarse and fine model design parameters by $\boldsymbol{x}_c$ and $\boldsymbol{x} \in \Re^{n\times 1}$, respectively. The corresponding response vectors are denoted by $\boldsymbol{R}_c$ and $\boldsymbol{R}_f \in \Re^{m\times 1}$, respectively.

We propose to find a mapping $\boldsymbol{P}$ relating the fine and coarse model parameters as

$$\boldsymbol{x}_c = \boldsymbol{P}(\boldsymbol{x}) \tag{12}$$

such that

$$\boldsymbol{R}_c(\boldsymbol{P}(\boldsymbol{x})) \approx \boldsymbol{R}_f(\boldsymbol{x}) \tag{13}$$

in a region of interest.

Then we can avoid using direct optimization, i.e., solving (1) to find $\boldsymbol{x}^*$. Instead, we declare $\bar{\boldsymbol{x}}$, given by

$$\bar{\boldsymbol{x}} \triangleq \boldsymbol{P}^{-1}(\boldsymbol{x}_c^*) \tag{14}$$

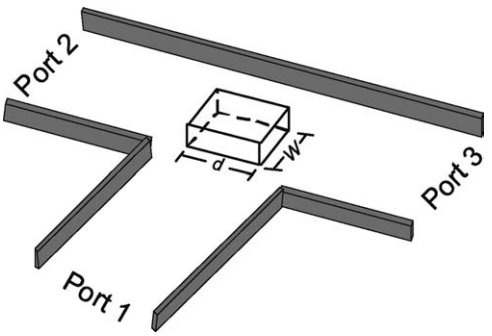

Figure 7 The loaded Tee junction.

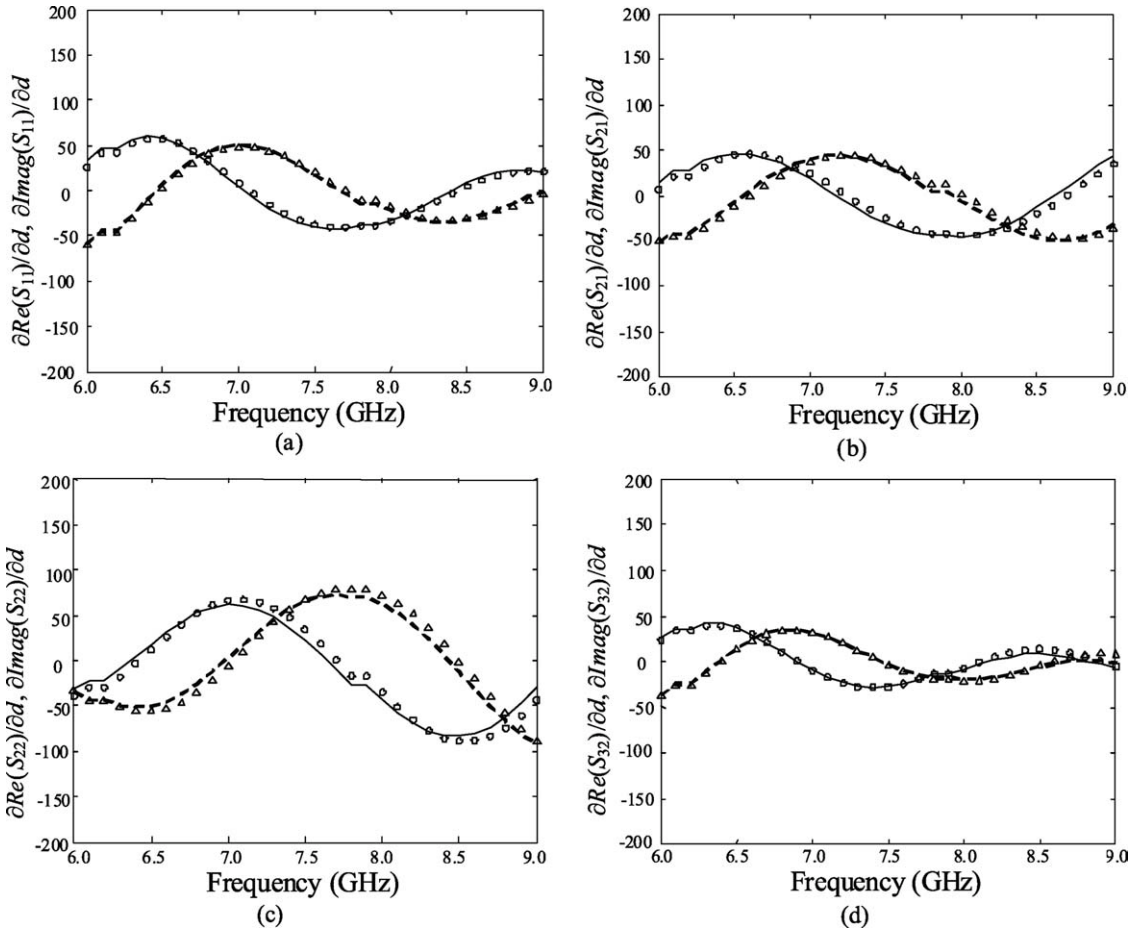

Figure 8 The sensitivities of the *S*-parameters for the loaded Tee junction over a sweep of frequencies for $[d\ W]^T = [4\Delta z\ 4\Delta x]^T$ with respect to *d*; sensitivities of the real part obtained through AVM (--); sensitivities of the real part obtained through forward differences (Δ); sensitivities of the imaginary part obtained through AVM (—); and sensitivities of the imaginary part obtained through forward differences (o).

as a good estimate of $\boldsymbol{x}^*$, where $\boldsymbol{x}_c^*$ is the result of coarse model optimization.

B. Interpretation of Space Mapping Optimization [53]

Space mapping algorithms initially optimize the coarse model to obtain the optimal design $\boldsymbol{x}_c^*$, for instance in the minimax sense. Subsequently, a mapped solution is found by minimizing the objective function $\|\boldsymbol{g}\|_2^2$, where $\boldsymbol{g}$ is defined by

$$\boldsymbol{g} = \boldsymbol{g}(\boldsymbol{x}) \stackrel{\Delta}{=} \boldsymbol{R}_f(\boldsymbol{x}) - \boldsymbol{R}_c(\boldsymbol{x}_c^*) \tag{15}$$

Correspondingly, according to [52], $\boldsymbol{R}_c(\boldsymbol{P}(\boldsymbol{x}))$ is optimized in the effort of finding a solution to (1). Here, $\boldsymbol{R}_c(\boldsymbol{P}(\boldsymbol{x}))$ is an expression of an ''enhanced'' coarse model or ''surrogate.'' Thus, the problem formulation (1) can be rewritten as

$$\bar{\boldsymbol{x}} = \arg\min_{\boldsymbol{x}} U(\boldsymbol{R}_c(\boldsymbol{P}(\boldsymbol{x}))) \tag{16}$$

where $\bar{x}$ may be close to $\boldsymbol{x}^*$ if $\boldsymbol{R}_c$ is close enough to $\boldsymbol{R}_f$. If $\boldsymbol{x}_c^*$ is unique then the solution of (16) is equivalent to driving the following residual vector $\boldsymbol{f}$ to zero:

$$\boldsymbol{f} = \boldsymbol{f}(\boldsymbol{x}) \stackrel{\Delta}{=} \boldsymbol{P}(\boldsymbol{x}) - \boldsymbol{x}_c^* \tag{17}$$

C. Original Space Mapping Approach [52, 53]

In this approach, an initial approximation of the mapping $\boldsymbol{P}^{(0)}$ is obtained by performing fine model analyses at a pre-selected set of at least m_0 base points, $m_0 \geq n+1$. One base point may be taken as the optimal coarse model solution, thus $\boldsymbol{x}^{(1)} = \boldsymbol{x}_c^*$. The remaining $m_0 - 1$ base points are chosen by perturbation. A corresponding set of coarse model points is then constructed through the parameter extraction process

$$\boldsymbol{x}_c^{(j)} \stackrel{\Delta}{=} \arg\min_{\boldsymbol{x}_c} \left\| \boldsymbol{R}_f(\boldsymbol{x}^{(j)}) - \boldsymbol{R}_c(\boldsymbol{x}_c) \right\| \tag{18}$$

for which

$$\begin{aligned} \varepsilon &\stackrel{\Delta}{=} \left\| \boldsymbol{R}_f(\boldsymbol{x}^{(j)}) - \boldsymbol{R}_c(\boldsymbol{x}_c^{(j)}) \right\| \\ &= \min_{\boldsymbol{x}_c} \left\| \boldsymbol{R}_f(\boldsymbol{x}^{(j)}) - \boldsymbol{R}_c(\boldsymbol{x}_c) \right\| \end{aligned} \tag{19}$$

is the parameter extraction error.

The additional $m_0 - 1$ points apart from $\boldsymbol{x}^{(1)}$ are required to establish full-rank conditions leading to the

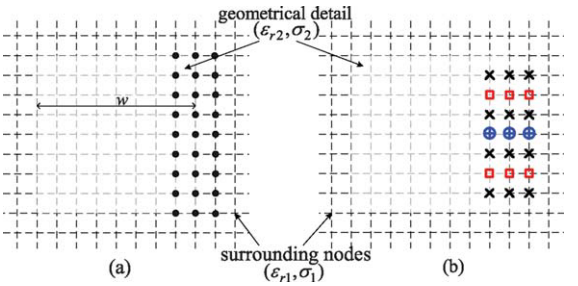

Figure 9 Sensitivity solver grid: (a) the fine simulation grid (b) the coarse sensitivity-analysis grids. [Color figure can be viewed in the online issue, which is available at wileyonlinelibrary.com.]

first mapping approximation $\boldsymbol{P}^{(0)}$. Bandler *et al.* [52] assumed a linear mapping between the two spaces, i.e.,

$$\boldsymbol{x}_c = \boldsymbol{P}^{(j)}(\boldsymbol{x}) = \boldsymbol{B}^{(j)}\boldsymbol{x} + \boldsymbol{c}^{(j)} \tag{20}$$

where $\boldsymbol{B}^{(j)} \in \Re^{n\times n}$ and $\boldsymbol{c}^{(j)} \in \Re^{n\times 1}$.

At the jth iteration, the sets of points in the two spaces may be expanded to contain, in general, m_j points which are used to establish the updated mapping $\boldsymbol{P}^{(j)}$. As the analytical form of $\boldsymbol{P}$ is not available, space mapping uses the current approximation $\boldsymbol{P}^{(j)}$, to estimate $\boldsymbol{x}^*$ at the jth iteration as

$$\bar{\boldsymbol{x}} \approx \boldsymbol{x}^{(m_j+1)} = (\boldsymbol{P}^{(j)})^{-1}(\boldsymbol{x}_c^*) \tag{21}$$

The process continues iteratively until $\boldsymbol{R}_f(\boldsymbol{x}^{(m_j+1)})$ is close enough to $\boldsymbol{R}_c(\boldsymbol{x}_c^*)$. If so, $\boldsymbol{P}^{(j)}$ is assumed close enough to our desired $\boldsymbol{P}$. If not, the set of base points in the fine space is augmented by $\boldsymbol{x}^{(m_j+1)}$, and $\boldsymbol{x}_c^{(m_j+1)}$, as determined by (18), augments the set of base points in the coarse space. Upon termination, we set the space-mapped design as in (21).

This algorithm is simple but has pitfalls. First, m_0 upfront high-cost fine model analyses are needed. Second, a linear mapping may not be valid for significantly misaligned models. Third, nonuniqueness in the parameter extraction process may lead to an erroneous mapping estimation and algorithm breakdown.

D. Aggressive Space Mapping Approach [53]

The aggressive space mapping algorithm incorporates a quasi-Newton iteration using the classical Broyden formula [71]. A rapidly improved design is anticipated following each fine model simulation, while the bulk of the computational effort (optimization, parameter extraction) is carried out in the coarse model space.

The aggressive space mapping technique iteratively solves the nonlinear system

$$\boldsymbol{f}(\boldsymbol{x}) = \boldsymbol{0} \tag{22}$$

for $\boldsymbol{x}$. Note, from (17), that at the jth iteration, the error vector $\boldsymbol{f}^{(j)}$ requires an evaluation of $\boldsymbol{P}^{(j)}(\boldsymbol{x}^{(j)})$. This is executed indirectly through the parameter extraction (evaluation of $\boldsymbol{x}_c^{(j)}$). Coarse model optimization produces $\boldsymbol{x}_c^*$.

The quasi-Newton step in the fine space is given by

$$\boldsymbol{B}^{(j)}\boldsymbol{h}^{(j)} = -\boldsymbol{f}^{(j)} \tag{23}$$

where $\boldsymbol{B}^{(j)}$, the approximation of the mapping Jacobian $\boldsymbol{J}_p$, is updated using Broyden's rank one update. Solving (23) for $\boldsymbol{h}^{(j)}$ provides the next iterate $\boldsymbol{x}^{(j+1)}$

$$\boldsymbol{x}^{(j+1)} = \boldsymbol{x}^{(j)} + \boldsymbol{h}^{(j)} \tag{24}$$

The algorithm terminates if $\|\boldsymbol{f}^{(j)}\|$ becomes sufficiently small. The output of the algorithm is an approximation to $\bar{\boldsymbol{x}} = \boldsymbol{P}^{-1}(\boldsymbol{x}_c^*)$ and the mapping matrix $\boldsymbol{B}$. The matrix $\boldsymbol{B}$ can be obtained in several ways, such as a unit mapping [72,

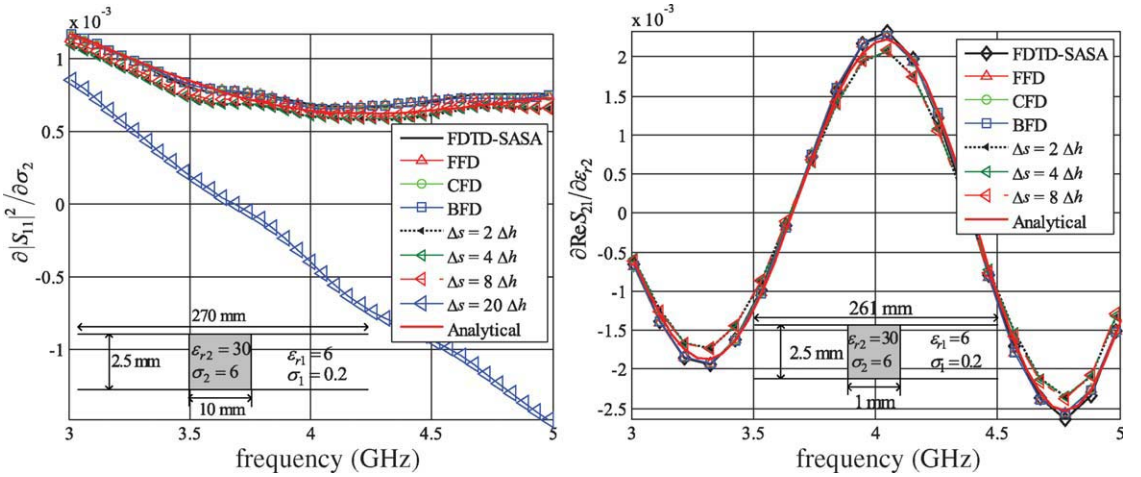

Figure 10 Sensitivity estimates obtained using the self adjoint approach (FDTD-SASA), using finite difference approaches, analytical approaches, and using different sampling rates of the field. Adjoint sensitivity analysis fails for the blue curve where the sampling rate drops below a quarter wavelength. [Color figure can be viewed in the online issue, which is available at wileyonlinelibrary.com.]

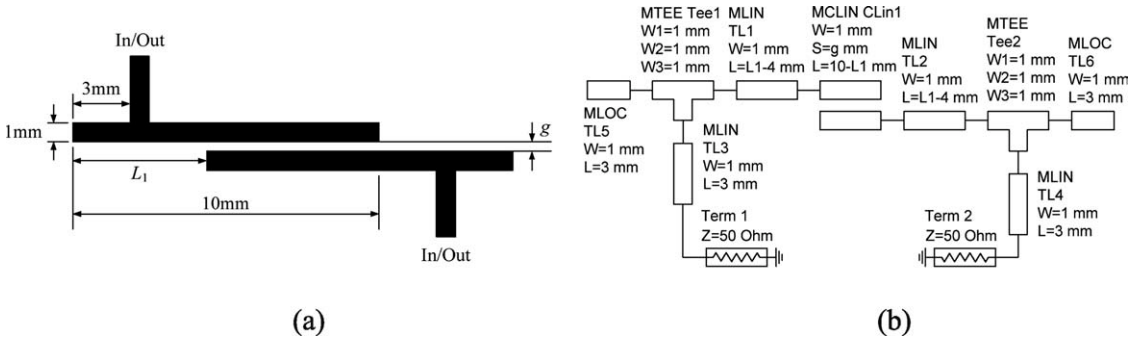

Figure 11 Second-order tapped-line microstrip filter [54, 79]: (a) geometry, (b) coarse model (Agilent ADS).

73], Broyden-like updates [70], Jacobian-based updates [53, 74], and constrained update [75].

E. General and Implicit Space Mapping [54]

Simple to implement, implicit space mapping [53, 76, 77], differs from earlier formulations in that the surrogate model parameters used for matching the fine model are separate from the design variables. Still, they are typically physically based and are usually selected and their values "preassigned" early in the modeling and design process. We have presented implicit space mapping for design optimization [76, 77] and device modeling [78, 79] tasks. Unlike input space mapping [53, 54], implicit space mapping does not affect the domain of the surrogate model whose parameters may be constrained. Most of our recent space mapping approaches can be generalized to a general space mapping form in the following procedure to solve (1)

$$\boldsymbol{x}^{(k+1)} = \arg\min_{\boldsymbol{x}} U(\boldsymbol{R}_s(\boldsymbol{x}, \boldsymbol{p}^{(k)})) \tag{25}$$

where $\boldsymbol{R}_s(\boldsymbol{x}, \boldsymbol{p})$ is a response vector of the space mapping surrogate model with $\boldsymbol{x}$ and $\boldsymbol{p}$ as design variables and model parameters, respectively. In implicit space mapping [76, 77], the model parameters are the so-called preassigned parameters. Parameters $\boldsymbol{p}^{(k)}$ are obtained at iteration k using the parameter extraction procedure

$$\boldsymbol{p}^{(k)} = \arg\min_{\boldsymbol{p}} \sum_{j=0}^{k} w_j ||\boldsymbol{R}_f(\boldsymbol{x}^{(k)}) - \boldsymbol{R}_s(\boldsymbol{x}^{(k)}, \boldsymbol{p})|| \tag{26}$$

where we try to match the surrogate with the fine model. Weighting factors w_j determine the contribution of previous iteration points to the parameter extraction process. The surrogate is usually the coarse model $\boldsymbol{R}_c$ composed with suitable transformations, e.g., the input space mapping surrogate is defined as a linear distortion of the coarse model domain: $\boldsymbol{R}_s(\boldsymbol{x}, \boldsymbol{p}) = \boldsymbol{R}_s(\boldsymbol{x}, \boldsymbol{B}, \boldsymbol{c}) = \boldsymbol{R}_c(\boldsymbol{B}\cdot\boldsymbol{x} + \boldsymbol{c})$.

Consider the second-order tapped-line microstrip filter [54, 76, 80] shown in Figure 11a. For simplicity we use two design parameters, L_1 and g as shown in Figure 11a. The fine model is simulated in FEKO [81]. The coarse model of Figure 11b is the circuit equivalent of the structure in Figure 11a, and is implemented in Agilent ADS [82].

We optimize our filter using implicit space mapping with the dielectric constant ε_r and height H of the substrate as preassigned parameters. Fixed in the fine model, we tune these parameters in the coarse model following our implicit space mapping steps.

The initial design is the optimal solution of the coarse model with respect to our specifications. Figure 12a shows the fine and coarse model responses at the initial design. Note that neither the coarse nor fine models satisfy the specifications. A significant misalignment is observed between them with respect to center frequency and bandwidth. We now perform the parameter extraction procedure and update ε_r and H so that the misalignment is minimized. Figure 12b shows the fine model and the

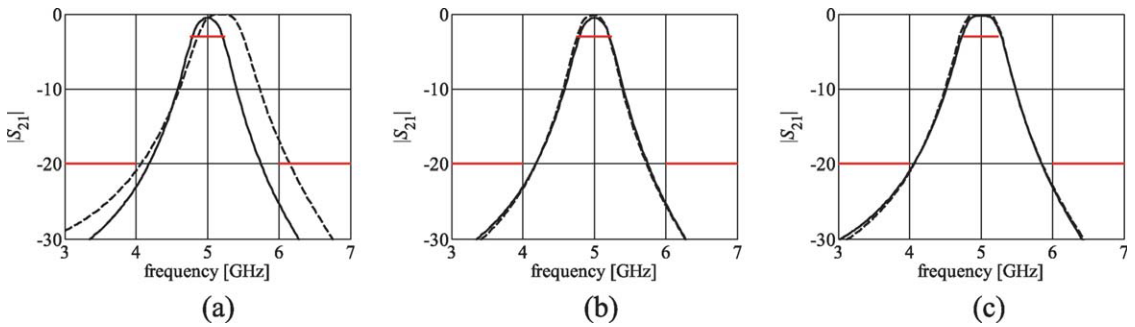

Figure 12 Second-order tapped-line microstrip filter [54, 79]: fine model (—) and coarse model (---) responses. (a) the initial design, (b) a good match obtained after extracting the preassigned parameters, (c) a good fine model response at the optimal design of the updated coarse model. [Color figure can be viewed in the online issue, which is available at wileyonlinelibrary.com.]

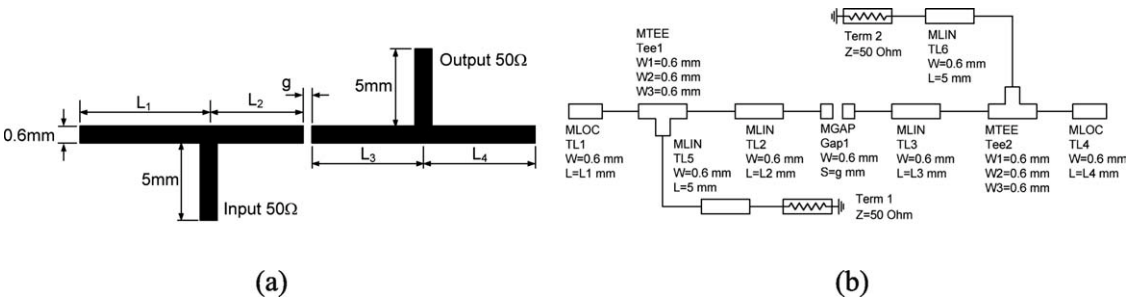

Figure 13 Microstrip bandpass filter [54, 83]: (a) geometry, (b) coarse model (Agilent ADS).

updated coarse model responses at the initial design. We (re)optimize the design parameters in our coarse model with the newly obtained preassigned parameter values. A new set of design values is found to update the fine model. The fine and coarse model responses at this new design are shown in Figure 12c. We observe that the fine model response satisfies the design specifications.

F. Output Space Mapping, Gradient-Based Space Mapping and Trust Region Methods [54]

The surrogate model is assumed to represent the fine model sufficiently well. A physically-based coarse model and a suitable combination of mappings provide a global match between the models. To achieve a more accurate local match, we proposed the so-called output space mapping [61, 83], which enhances the (original) surrogate by a correction term. Its simplest correction is the difference between the fine and the original space mapping responses at the current iteration point so that a perfect match between these models is ensured (also called zero-order consistency [64]).

Consider the microstrip bandpass filter shown in Figure 13a [84]. The fine model is implemented in FEKO, the coarse model is a circuit equivalent implemented in Agilent ADS (Fig. 13b). Figure 14a shows the fine model (solid line) and the (frequency) space mapping surrogate (dashed line) responses at, say, iteration *i*. Figure 14b shows the response of the optimized surrogate model as well as the fine model response at the surrogate model optimum. If the surrogate model is enhanced by the output space mapping term, its response becomes identical to the fine model response of Figure 14a. Optimizing this enhanced model, we obtain the responses of Figure 14c, and we see that the fine model response of Figure 14c is better than that of Figure 14b with respect to the given specification. Thus, the output space mapping correction compensates the misalignment between the fine and surrogate models (Fig. 14a) and, although the alignment is perfect only at the current design, it also reduces mismatches between the models in the neighbourhood of this design.

The surrogate model can be further enhanced by an additional linear term, which ensures coincidence of the Jacobian of the surrogate and the Jacobian of the fine model at the current design [61] (first-order consistency condition [64]). This term requires a fine model sensitivity analysis, however, it is more robust and ensures the convergence of the algorithm to a local fine model optimum if the algorithm is safeguard by trust region methods [62]. Theoretical aspects of the output and gradient-based space mapping are discussed in [61].

G. The Tuning Space Mapping Algorithm [55]

The tuning space mapping procedure encompasses the port tuning method proposed for design using EM simulators [85]. We define multiple auxiliary ports within a structure, e.g., in the manner of the ''cocalibrated'' [86] internal ports of Sonnet ***em*** [87]. We call this structure with defined internal ports ''auxiliary fine model.''

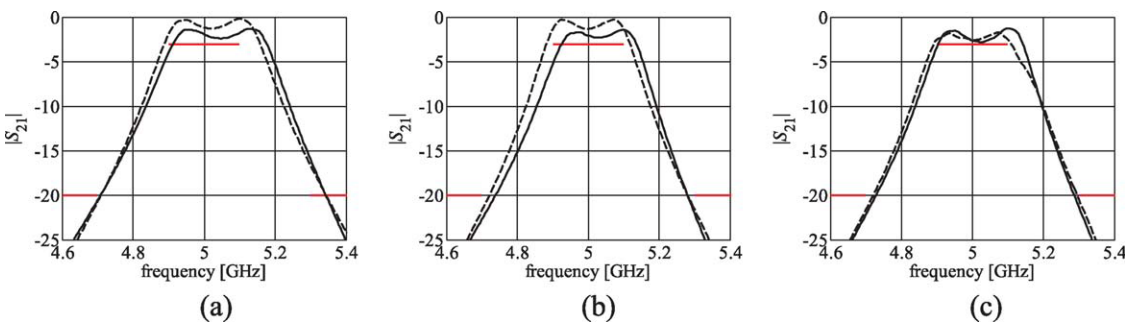

Figure 14 Fine model (solid line) and surrogate model (dashed) responses for the microstrip bandpass filter [54, 83]: (a) the fine and surrogate model responses at iteration *i*, (b) the response of the optimized surrogate and fine model responses at the surrogate model optimum, (c) the response of the optimized surrogate enhanced by output space mapping and the fine model response at the enhanced surrogate model optimum (fine model specification error +0.4 dB). [Color figure can be viewed in the online issue, which is available at wileyonlinelibrary.com.]

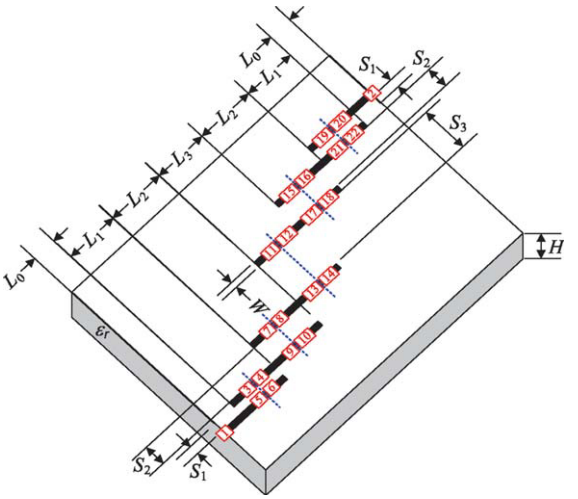

Figure 15 HTS filter: physical structure with tuning ports [88]. [Color figure can be viewed in the online issue, which is available at wileyonlinelibrary.com.]

Elements can then be incorporated into the auxiliary fine model to form a tuning model. Tuning space mapping techniques [55, 88–91] utilize tuning model as surrogate. The resulting tunable model constitutes a surrogate for design or modeling purposes.

In [87, 88], tuning space mapping involves a so-called ''Type 0'' embedding, in which tuning elements are attached to internal ports of the fine model. If a tuning-to-design-parameter conversion is not available, we require for calibration purposes an additional full-system coarse model or the simulation of a perturbed fine model.

In [55, 89], we replace certain designable sub-section(s) with so-called ''Type 1'' tuning element(s). In most of our examples, these elements have direct tuning parameters, i.e., distributed microwave circuit elements with physical dimensions corresponding to those of the fine model. In a simple parameter extraction procedure, we match the tuning model with the fine model (the original structure without internal ports). We assume that certain fine-model couplings are preserved in the tuning model. Thereby, we expect to obtain a good surrogate of the fine model that is subsequently tuned to satisfy our goals by optimizing its tuning parameters. The obtained tuning parameter values are converted to design parameter values that become our next fine model iterate (design).

Our algorithm produces a sequence of points (design variable vectors) $\boldsymbol{x}^{(i)}$, $i = 0, 1, \ldots$. The iteration of the algorithm consists of three steps: 1) alignment of the tuning model with the fine model, 2) the optimization of the tuning model, and 3) the calibration of the tuning parameters to the design parameters.

In our first step, based on data from the fine model (with internal ports) at point $\boldsymbol{x}^{(i)}$, the current tuning model $\boldsymbol{R}_s^{(i)}$ is built with appropriate Type 0 or Type 1 embedding. The tuning model response may not agree with the response of the original fine model $\boldsymbol{R}_f$ at $\boldsymbol{x}^{(i)}$. We align these models by the procedure

$$(\boldsymbol{x}_p^{(i)}, \boldsymbol{t}_0^{(i)}) = \arg\min_{\boldsymbol{x}_p, \boldsymbol{t}_0} \left\| \boldsymbol{R}_f(\boldsymbol{x}^{(i)}) - \boldsymbol{R}_t^{(i)}(\boldsymbol{t}_0, \boldsymbol{x}_p) \right\| \tag{27}$$

where $\boldsymbol{R}_t \in R^m$ denotes the response vector of the tuning model, $\boldsymbol{x}_p$ represents the preassigned parameters of the tuning model, and $\boldsymbol{t}_0$ represents the initial tuning parameters of the tuning model. We may only need to extract either $\boldsymbol{t}_0$ or $\boldsymbol{x}_p$ depending on the type of tuning model.

In the second step, we optimize $\boldsymbol{R}_t^{(i)}$ to have it meet the design specifications. We obtain the optimal values of the tuning parameter $\boldsymbol{t}_1^{(i)}$ as

$$\boldsymbol{t}_1^{(i)} = \arg\min_{\boldsymbol{t}_1} U\left(\boldsymbol{R}_t^{(i)}(\boldsymbol{t}_1, \boldsymbol{x}_p^{(i)})\right) \tag{28}$$

Having $\boldsymbol{t}_1^{(i)}$ we perform the calibration procedure to determine the values of the design variables that yield the same change in the tuning model response as $\boldsymbol{t}_0^{(i)}$ goes to $\boldsymbol{t}_1^{(i)}$.

The new design is obtained through the calibration step [88]

$$\boldsymbol{x}^{(i+1)} = \boldsymbol{x}^{(i)} + \boldsymbol{s}^{(i)} * \left(\boldsymbol{t}_1^{(i)} - \boldsymbol{t}_0^{(i)}\right) \tag{29}$$

where $\boldsymbol{s}^{(i)}$ is a real vector and * denotes component-wise multiplication. For direct tuning elements, $\boldsymbol{s}^{(i)} = [1\ 1\ \ldots\ 1]^T$. Otherwise a calibration step [88] follows to calculate $\boldsymbol{s}^{(i)}$.

Figure 15 shows the structure of a high-temperature superconducting (HTS) filter [88]. The design parameters are the lengths of the coupled-line sections and the spacing between them, shown as L_1, L_2, L_3, S_1, S_2, and S_3, respectively.

The tuning model is constructed by dividing the five coupled-line polygons in the middle and inserting the tuning ports at the new cut edges. Its S22P data file (22 being the number of ports) is then loaded into the S-parameter component in Agilent ADS. The circuit-theory coupled-line components and capacitor components are chosen to be the tuning elements and are inserted into each pair of tuning ports (Fig. 16). The lengths of the additional coupled-lines and the capacitances of the capacitors are

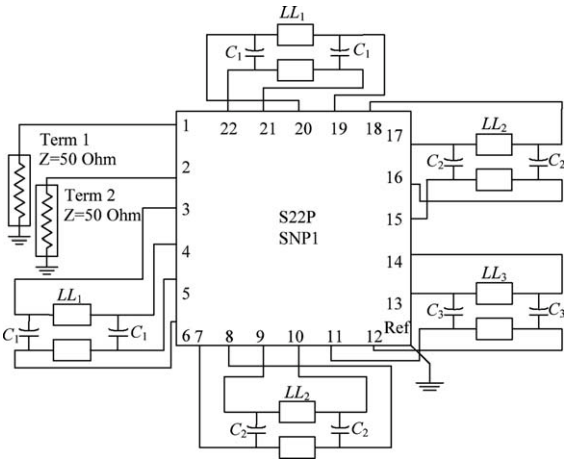

Figure 16 HTS filter: tuning model (Agilent ADS) [88].

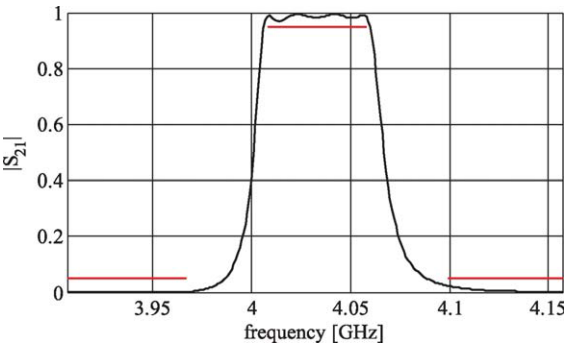

Figure 17 HTS filter: fine model response ($|S_{21}|$ obtained with Sonnet ***em***) at the final design. [Color figure can be viewed in the online issue, which is available at wileyonlinelibrary.com.]

assigned as tuning parameters, so that we have $\boldsymbol{x}_t = [LL_1\ LL_2\ LL_3\ C_1\ C_2\ C_3]^T$ (LL_k in mm, C_k in pF).

The calibration model implemented in ADS is an equivalent circuit containing the same tuning elements as the tuning model. It mimics the division of the coupled lines in preparing $\boldsymbol{R}_t$. The calibration model also contains six (implicit) space mapping parameters to be used as parameters $\boldsymbol{p}$ in the calibration process [88], namely, $\boldsymbol{p} = [H_1\ H_2\ H_3\ \varepsilon_{r1}\ \varepsilon_{r2}\ \varepsilon_{r3}]^T$, where H_k and ε_{rk} are substrate height and dielectric constant of the coupled-line segment of length L_k according to Figure 15.

The initial design $\boldsymbol{x}^{(0)}$ is the optimal solution of the coarse model, i.e., the calibration model with zero values for the tuning parameters.

Figure 17 shows the fine model response at $\boldsymbol{x}^{(2)}$. Note that the tuning space mapping algorithm requires only one iteration to satisfy the design specifications, and only one additional iteration to obtain an almost equal-ripple fine model response.

H. Building a Surrogate

Building a surrogate may not be straightforward. We show, using the microstrip-fed monopole antenna [92] of Figure 18, how to combine functional and physical models in building a surrogate.

Our design variables are $\boldsymbol{x} = [W_{p1}\ L_{p1}\ L_{p2}\ W_{g2}\ L_{p0}]^T$. The remaining parameters are fixed. The fine model of the

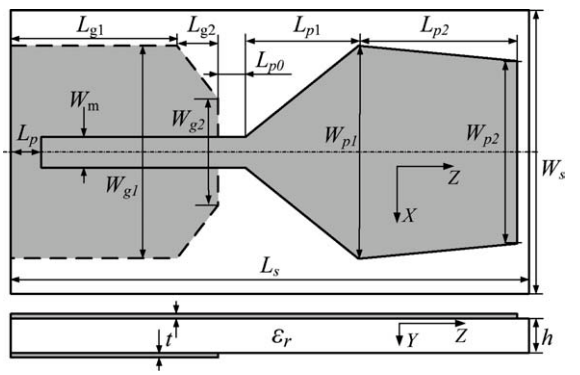

Figure 18 Microstrip-fed planar monopole antenna [91].

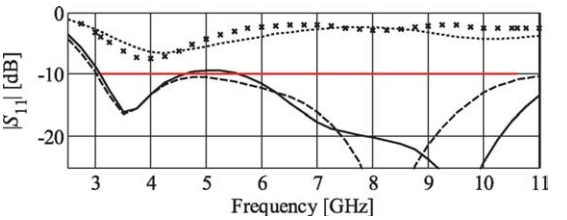

Figure 19 The microstrip-fed monopole antenna: fine model (dotted line) and coarse model (×) responses at the initial design $\boldsymbol{x}^{\text{init}}$, as well as the fine model (solid line) and coarse model (dashed line) responses at the coarse model optimum $\boldsymbol{x}^{(0)}$. [Color figure can be viewed in the online issue, which is available at wileyonlinelibrary.com.]

antenna is evaluated by CST Microwave Studio (simulation time about 2.5 h). The design specifications are $|S_{11}| \leq -10$ dB for 3.1 to 10.6 GHz. We want to optimize the antenna using space mapping, however, a suitable equivalent-circuit coarse model is not available. Instead, we use a coarse-discretization CST model $\boldsymbol{R}_{cd}$ (evaluation time 2 min and 15 sec). $\boldsymbol{R}_{cd}$ is still computationally too expensive to be used directly as a coarse model, therefore, a coarse model $\boldsymbol{R}_c$ is created in the neighbourhood of the starting point (here, the approximate optimum of $\boldsymbol{R}_{cd}$), using kriging interpolation [58] of the $\boldsymbol{R}_{cd}$ data. The procedure is as follows.

1. Allocate N base designs, $X_B = \{\boldsymbol{x}^1, \ldots, \boldsymbol{x}^N\}$, using Latin Hypercube Sampling [93];
2. Evaluate $\boldsymbol{R}_{cd}$ at each design $\boldsymbol{x}^j$, $j = 1, 2, \ldots, N$;
3. Build $\boldsymbol{R}_c$ as a kriging interpolation of data pairs $\{(\boldsymbol{x}^j, \boldsymbol{R}_{cd}(\boldsymbol{x}^j))\}_{j\ =\ 1,\ldots,N}$.

The coarse model created this way is computationally cheap, easy to optimize, and yet retains the features of a physically-based model. The initial design is $\boldsymbol{x}^{\text{init}} = [19\ 0\ 17\ 22.5\ 0]^T$ mm. The starting point for space mapping optimization, $\boldsymbol{x}^{(0)} = [20.33\ 2.44\ 19\ 15.17\ 0]^T$ mm, is the approximate optimum of $\boldsymbol{R}_{cd}$. The kriging coarse model $\boldsymbol{R}_c$ is set up in the region defined by deviation $\delta = [2\ 1\ 2\ 1\ 0.5]^T$ mm from $\boldsymbol{x}^{(0)}$ using $N = 100$ base points. Figure 19 shows the responses of $\boldsymbol{R}_f$ and $\boldsymbol{R}_c$ at both $\boldsymbol{x}^{\text{init}}$ and $\boldsymbol{x}^{(0)}$. The space mapping algorithm uses the input/output space mapping surrogate $\boldsymbol{R}_s = \boldsymbol{R}_c(\boldsymbol{x} + \boldsymbol{c}) + \boldsymbol{d}$. The design after three evaluations of $\boldsymbol{R}_f$ is $\boldsymbol{x}^* = [20.2\ 2.27\ 19.5\ 14.77\ 0.384]^T$ mm. The fine model specification error at $\boldsymbol{x}^*$ is –

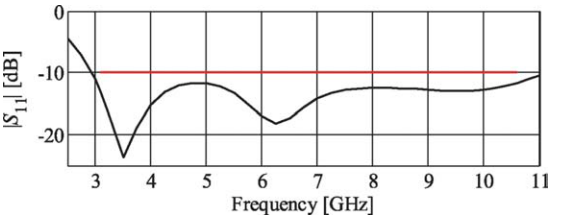

Figure 20 The microstrip-fed monopole: fine model $|S_{11}|$ at the final design. [Color figure can be viewed in the online issue, which is available at wileyonlinelibrary.com.]

TABLE I Microstrip-Fed Monopole Antenna: Optimization Cost

Algorithm Component	Number of Model Evaluations	CPU Time	
		Absolute	Relative to $\boldsymbol{R}_f$
Optimizing $\boldsymbol{R}_{cd}$	$145 \times \boldsymbol{R}_{cd}$	5 h 25 min	2.3
Setting up $\boldsymbol{R}_c$	$100 \times \boldsymbol{R}_{cd}$	3 h 43 min	1.6
Evaluation of $\boldsymbol{R}_f$	$4 \times \boldsymbol{R}_f$	9 h 30 min	4.0
Total cost*	N/A	18 h 38 min	7.9

2.1 dB (Fig. 20). The total optimization time (Table I) corresponds to only about eight evaluations of $\boldsymbol{R}_f$.

VI. CONCLUSIONS

We briefly review the history of microwave CAD and recent developments high-performance EM-based design optimization. We describe two state-of-the-art approaches in EM-based optimization and modeling, namely, adjoint sensitivity analysis and space mapping. They dramatically improve the efficiency of EM optimization. We illustrate the techniques with applications and examples. We believe that combining space mapping with adjoint sensitivity evaluation should form the next generation of effective space mapping algorithms.

ACKNOWLEDGMENT

We thank Sonnet Software, Inc., Syracuse, NY, for ***em***™, CST AG, Darmstadt, Germany, for CST Microwave Studio, and Agilent Technologies, Santa Rosa, CA, for ADS. J.W. Bandler is also with Bandler Corporation, Dundas, ON, Canada. This work was supported in part by the Natural Sciences and Engineering Research Council of Canada under Grants OGP0007239 and STPGP381153, by Bandler Corporation, and by the Reykjavik University Development Fund under Grant T09009.

REFERENCES

1. G.C. Temes and D.A. Calahan, Computer-aided network optimization the state-of-the-art, Proc IEEE 55 (1967), 1832–1863.
2. J.W. Bandler, Optimization methods for computer-aided design, IEEE Trans Microwave Theory Tech, 17 (1975), 533–552; Appears in Microwave Integrated Circuits, J Frey Ed, Artech House, 1975.
3. J.W. Bandler, Computer-aided circuit optimization, in G.C. Temes and S.K. Mitra, Eds., Modern Filter Theory and Design, Wiley, New York, 1973, pp. 211–271.
4. G.E. Brehm, Multifunction MMIC history from a process technology perspective, IEEE Trans Microwave Theory Tech 38 (1990), pp. 1164–1170.
5. J.W. Bandler, S.H. Chen, S. Daijavad, W. Kellermann, M. Renault, and Q.J. Zhang, Large scale minimax optimization of microwave multiplexers, Proc European Microwave Conf, Dublin, Ireland, 1986, 435–440.
6. J.W. Bandler, R.M. Biernacki, Q. Cai, S.H. Chen, S. Ye, and Q.J. Zhang, Integrated physics-oriented statistical modeling, simulation and optimization, IEEE Trans Microwave Theory Tech 40 (1992), 1374–1400.
7. J.W. Bandler and S.H. Chen, Circuit optimization: The state of the art, IEEE Trans Microwave Theory Tech 36 (1988), 424–443.
8. J.W. Bandler and A.E. Salama, Functional approach to microwave postproduction tuning, IEEE Trans Microwave Theory Tech 33 (1985), 302–310.
9. Available at http://www.microwaves101.com. Accessed on March 5, 2010.
10. OSA90/hope™, HarPE™, Empipe™, Empipe3D™, version 4.0, User's Manual, August 1997, Optimization Systems Associates Inc. (now Agilent Technologies), Dundas, Ontario, Canada.
11. J.W. Bandler, P.C. Liu, and H. Tromp, A nonlinear programming approach to optimal design centering, tolerancing and tuning, IEEE Trans Circuits Syst 23 (1976), 155–165.
12. J.W. Bandler, R.M. Biernacki, S.H. Chen, P.A. Grobelny, and S. Ye, Yield-driven electromagnetic optimization via multilevel multidimensional models, IEEE Trans Microwave Theory Tech 41 (1993), 2269–2278.
13. J.W. Bandler, R.M. Biernacki, and S.H. Chen, Parameterization of arbitrary geometrical structures for automated electromagnetic optimization, Int J RF Microwave CAE 9 (1999), 73–85.
14. J.W. Bandler, R.M. Biernacki, S.H. Chen, D.G. Swanson Jr., and S. Ye, Microstrip filter design using direct EM field simulation, IEEE Trans Microwave Theory Tech 42 (1994), 1353–1359.
15. J.W. Bandler, R.M. Biernacki, S.H. Chen, W.J. Getsinger, P.A. Grobelny, C. Moskowitz, and S.H. Talisa, Electromagnetic design of high-temperature superconducting microwave filters, Int J Microwave Millimet Wave Comput Aid Eng 5 (1995), 331–343.
16. J.W. Bandler, R.M. Biernacki, S.H. Chen, L.W. Hendrick, and D. Omeragić, Electromagnetic optimization of 3-D structures, IEEE Trans Microwave Theory Tech 45 (1997), 770–779.
17. D.G. Swanson Jr., Optimizing a microstrip bandpass filter using electromagnetics, Int J Microwave Millimet Wave Comput Aided Eng 5 (1995), 344–351.
18. J.W. Bandler and M. Mongiardo, Guest editorial electromagnetics-based optimization of microwave components and circuits, IEEE Trans Microwave Theory Tech 52 (2004), 241–244.
19. D. De Zutter, J. Sercu, T. Dhaene, J. De Geest, F.J. Demuynck, S. Hammadi, and C.-W. Paul, Recent trends in the integration of circuit optimization and full-wave electromagnetic analysis, IEEE Trans Microwave Theory Tech 52 (2004), 245–256.
20. J.C. Rautio, A conformal mesh for efficient planar electromagnetic analysis, IEEE Trans Microwave Theory Tech 52 (2004), 257–264.
21. M. Mattes and J.R. Mosig, A novel adaptive sampling algorithm based on the survival-of-the-fittest principle of genetic algorithms, IEEE Trans Microwave Theory Tech 52 (2004), 265–275.
22. Y.A. Hussein and S.M. El-Ghazaly, Modeling and optimization of microwave devices and circuits using genetic algorithms, IEEE Trans Microwave Theory Tech 52 (2004), 329–336.
23. S.W. Director and R.A. Rohrer, The generalized adjoint network and network sensitivities, IEEE Trans Circuit Theory CT-16 (1969), 318–323.
24. S.W. Director and R.A. Rohrer, Automated network design—the frequency-domain case, IEEE Trans Circuit Theory CT-16 (1969), 330–337.
25. J.W. Bandler and R.E. Seviora, Direct method for evaluating scattering matrix sensitivities, Electron Lett 6 (1970), 773–774.
26. J.W. Bandler and R.E. Seviora, Current trends in network optimization, IEEE Trans Microwave Theory Tech 18 (1970), 1159–1170.

27. J.W. Bandler and R.E. Seviora, Computation of sensitivities for non-commensurate networks, IEEE Trans Circuit Theory, 18 (1971), 174–178.
28. J.W. Bandler and R.E. Seviora, Wave sensitivities of networks, IEEE Trans Microwave Theory Tech 20 (1972), 138–147.
29. Y.S. Chung, C. Cheon, I.H. Park, and S.Y. Hahn, Optimal design method for microwave device using time domain method and design sensitivity analysis-part II: FDTD case, IEEE Trans Magn 37 (2001), 3255–3259.
30. M.H. Bakr and N.K. Nikolova, An adjoint variable method for time domain TLM with fixed structured grids, IEEE Trans Microwave Theory Tech 52 (2004), 554–559.
31. M.H. Bakr and N.K. Nikolova, An adjoint variable method for time domain TLM with wideband Johns matrix boundaries, IEEE Trans Microwave Theory Tech 52 (2004), 678–685.
32. M.H. Bakr and N.K. Nikolova, Efficient estimation of adjoint-variable S-parameter sensitivities with time domain TLM, Int J Numerical Modell 18 (2005), 171–187.
33. M.H. Bakr, N.K. Nikolova, and P.A.W. Basl, Self-adjoint S-parameter sensitivities for lossless homogeneous TLM problems, Int J Numer Modell 18 (2005), 441–455.
34. P.A.W. Basl, M.H. Bakr, and N.K. Nikolova, Theory of self-adjoint S-parameter sensitivities for lossless nonhomogeneous transmission-line modeling problems, IET Microwave Antennas Propag 2 (2008), 211–220.
35. N.K. Nikolova, H.W. Tam, and M.H. Bakr, Sensitivity analysis with the FDTD method on structured grids, IEEE Trans Microwave Theory Tech 52 (2004), 1207–1216.
36. N.K. Nikolova, Ying Li, Yan Li, and M.H. Bakr, Sensitivity analysis of scattering parameters with electromagnetic time-domain simulators, IEEE Trans Microwave Theory Tech 54 (2006), 1598–1610.
37. Y. Song, N.K. Nikolova, and M.H. Bakr, Efficient time-domain sensitivity analysis using coarse grids, Appl Comput Electromagn Soc J 23 (2008), 5–15.
38. Y. Song and N.K. Nikolova, Memory efficient method for wideband self-adjoint sensitivity analysis, IEEE Trans Microwave Theory Tech 56 (2008), 1917–1927.
39. J.P. Webb, Design sensitivity of frequency response in 3-D finite-element analysis of microwave devices, IEEE Trans Magn 38 (2002), 1109–1112.
40. D. Nair and J.P. Webb, Optimization of microwave devices using 3-D finite elements and the design sensitivity of the frequency response, IEEE Trans Magn 39 (2003), 1325–1328.
41. N.K. Georgieva, S. Glavic, M.H. Bakr, and J.W. Bandler, Feasible adjoint sensitivity technique for EM design optimization, IEEE Trans Microwave Theory Tech 50 (2002), 2751–2758.
42. N.K. Nikolova, J.W. Bandler, and M.H. Bakr, Adjoint techniques for sensitivity analysis in high-frequency structure CAD, IEEE Trans Microwave Theory Tech 52 (2004), 403–419.
43. E.A. Soliman, M.H. Bakr, and N.K. Nikolova, An adjoint variable method for sensitivity calculations of multiport devices, IEEE Trans Microwave Theory Tech 52 (2004), 589–599.
44. S.M. Ali, N.K. Nikolova, and M.H. Bakr, Sensitivity analysis with full-wave EM solvers based on structured grids, IEEE Trans Magn 40 (2004), 1521–1529.
45. S.M. Ali, N.K. Nikolova, and M.H. Bakr, Recent advances in sensitivity analysis with frequency-domain full-wave EM solvers, Appl Comput Electromagn Soc J 19 (2004), 147–154.
46. M.A. El Sabbagh, M.H. Bakr, and N.K. Nikolova, Sensitivity analysis of the scattering parameters of microwave filters using the adjoint network method, Int J RF Microwave Comput-Aid Eng 16 (2006), 596–606.
47. M.A. El Sabbagh, M.H. Bakr, and J.W. Bandler, Adjoint higher-order sensitivities for fast full-wave optimization of microwave filters, IEEE Trans Microwave Theory Tech 54 (2006), 3339–3351.
48. M. A. Swillam, M. H. Bakr, and X. Li, Efficient Adjoint sensitivity analysis exploiting the FD-BPM, IEEE J Lightwave Technol 25 (2007), 1861–1869.
49. A. Dounavis, E. Gad, R. Achar, and M.S. Nakhla, Passive model reduction of multiport distributed interconnects, IEEE Trans Microwave Theory Tech 48 (2000), 2325–2334.
50. A.H. Zaabab, Q.J. Zhang, and M.S. Nakhla, A neural network modeling approach to circuit optimization and statistical design, IEEE Trans Microwave Theory Tech 43 (1995), 1349–1358.
51. N.V. Queipo, R.T. Haftka, W. Shyy, T. Goel, R. Vaidyanathan, and P.K. Tucker, Surrogate-based analysis and optimization, Prog Aerosp Sci 41 (2005), 1–28.
52. J.W. Bandler, R.M. Biernacki, S.H. Chen, P.A. Grobelny, and R.H. Hemmers, Space mapping technique for electromagnetic optimization, IEEE Trans Microwave Theory Tech 42 (1994), 2536–2544.
53. J.W. Bandler, Q.S. Cheng, S.A. Dakroury, A.S. Mohamed, M.H. Bakr, K. Madsen, and J. Søndergaard, Space mapping: the state of the art, IEEE Trans Microwave Theory Tech 52 (2004), 337–361.
54. S. Koziel, Q.S. Cheng, and J.W. Bandler, Space mapping, IEEE Microwave Mag 9 (2008), 105–122.
55. Q.S. Cheng, J.W. Bandler, and S. Koziel, Space mapping design framework exploiting tuning elements, IEEE Trans. Microwave Theory Tech 58 (2010), 136–144.
56. J. Søndergaard, Optimization using surrogate models, Ph.D. thesis, Informatics and Mathematical Modeling, Technical University of Denmark, Lyngby, Denmark, 2003.
57. M.D. Buhmann and M.J. Ablowitz, Radial Basis Functions: Theory and Implementations, Cambridge University, Cambridge, UK, 2003.
58. T.W. Simpson, T.M. Maurey, J.J. Korte, and F. Mistree, Kriging models for global approximation in simulation-based multidisciplinary design optimization, AIAA J 39 (2001), 2233–2241.
59. A.J. Smola and B. Schölkopf, A tutorial on support vector regression, Stat Comput 14 (2004), 199–222.
60. L. Zhang, J. Xu, M.C.E. Yagoub, R. Ding, and Q.-J. Zhang, Efficient analytical formulation and sensitivity analysis of neuro-space mapping for nonlinear microwave device modeling, IEEE Trans Microwave Theory Tech 53 (2005), 2752–2767.
61. S. Koziel, J.W. Bandler, and K. Madsen, A space mapping framework for engineering optimization: Theory and implementation, IEEE Trans Microwave Theory Tech 54 (2006), 3721–3730.
62. A.R. Conn, N.I.M. Gould, and P.L. Toint, Trust Region Methods, MPS-SIAM Series on Optimization, Society for Industrial and Applied Mathematics, Philadelphia, PA, USA, 2000.
63. N.M. Alexandrov, J. E. Dennis, R. M. Lewis, and V. Torczon, A trust region framework for managing use of approximation models in optimization, Struct Multidisciplinary Optim 15 (1998), 16–23.
64. D. Echeverria and P.W. Hemker, Space mapping and defect correction, CMAM, Int Math J. Comput Meth Appl Math 5 (2005), 107–136.
65. T. Robinson, M. Eldred, K. Willcox, and R. Haimes, Surrogate-based optimization using multifidelity models with variable parameterization and corrected space mapping, AIAA J 46 (2008), 2814–2822.

66. N.M. Alexandrov and R.M. Lewis, An overview of first-order model management for engineering optimization, Optim Eng 2 (2001), 413–430.
67. A.J. Booker, J.E. Dennis Jr., P.D. Frank, D.B. Serafini, V. Torczon, and M.W. Trosset, A rigorous framework for optimization of expensive functions by surrogates, Struct Optim 17 (1999), 1–13.
68. S.J. Leary, A. Bhaskar, and A.J. Keane, A knowledge-based approach to response surface modeling in multifidelity optimization, J Global Optim 26 (2003), 297–319.
69. Y.S. Ong, P.B. Nair, and A.J. Keane, Evolutionary optimization of computationally expensive problems via surrogate modeling, AIAA J 41 (2003), 687–696.
70. M.H. Bakr, P.P.M. So, and W.J.R. Hoefer, The generation of optimal microwave topologies using time-domain field synthesis, IEEE Trans Microwave Theory Tech 50 (2002), 2537–2544.
71. C.G. Broyden, A class of methods for solving nonlinear simultaneous equations, Math Comp 19 (1965), 577–593.
72. S. Bila, D. Baillargeat, S. Verdeyme, and P. Guillon, Automated design of microwave devices using full EM optimization method, IEEE MTT-S Int Microwave Symp Dig, Baltimore, MD, June1998, pp. 1771–1774.
73. A.M. Pavio, The electromagnetic optimization of microwave circuits using companion models, Workshop on Novel Methodologies for Device Modeling and Circuit CAD, IEEE MTT-S Int Microwave Symp Dig, Anaheim, CA, 1999.
74. J.W. Bandler, S.H. Chen, S. Daijavad, and K. Madsen, Efficient optimization with integrated gradient approximations, IEEE Trans Microwave Theory Tech 36 (1988), 444–455.
75. M.H. Bakr, J.W. Bandler, K. Madsen, and J. Søndergaard, Review of the space mapping approach to engineering optimization and modeling, Optim Eng 1 (2000), 241–276.
76. J.W. Bandler, Q.S. Cheng, N.K. Nikolova, and M.A. Ismail, Implicit space mapping optimization exploiting preassigned parameters, IEEE Trans Microwave Theory Tech 52 (2004), 378–385.
77. Q.S. Cheng, J.W. Bandler, and S. Koziel, Combining coarse and fine models for optimal design, IEEE Microwave Mag 9 (2008), 79–88.
78. Q.S. Cheng and J.W. Bandler, An implicit space mapping technique for component modeling, in Proc. 36th European Microwave Conf., Manchester, UK, Sep.2006, pp. 458–461.
79. Q.S. Cheng, S. Koziel, and J.W. Bandler, Simplified space-mapping approach to enhancement of microwave device models, Int J RF Microwave Comput-Aid Eng 16 (2006), 518–535.
80. A. Manchec, C. Quendo, J.-F. Favennec, E. Rius, and C. Person, Synthesis of capacitive-coupled dual-behavior resonator (CCDBR) filters, IEEE Trans Microwave Theory Tech 54 (2006), 2346–2355.
81. FEKO User's Manual, Suite 5.3, 2008, EM Software & Systems-S.A. (Pty) Ltd, 32 Techno Lane, Technopark, Stellenbosch, 7600, South Africa, Available at http://www.feko.info.
82. Agilent ADS, Version 2009, Agilent Technologies, Palo Alto, CA, 94304, 2009.
83. J.W. Bandler, Q.S. Cheng, D.H. Gebre-Mariam, K. Madsen, F. Pedersen, and J. Søndergaard, EM-based surrogate modeling and design exploiting implicit, frequency and output space mappings, IEEE MTT-S Int Microwave Symp Dig, Philadelphia, PA, June 2003, pp. 1003–1006.
84. A. Hennings, E. Semouchkina, A. Baker, and G. Semouchkin, Design optimization and implementation of bandpass filters with normally fed microstrip resonators loaded by high-permittivity dielectric, IEEE Trans Microwave Theory Tech 54 (2006), 1253–1261.
85. D.G. Swanson, Fast analysis and optimization of combline filters using FEM, IEEE MTT-S Int. Microwave Symp. Dig., Phoenix, AZ, May 2001, pp. 1159–1162.
86. J.C. Rautio, Perfectly calibrated internal ports in EM analysis of planar circuits, IEEE MTT-S Int Microwave Symp Dig, Atlanta, GA, June 2008, pp. 1373–1376.
87. Sonnet ***em***, Ver. 12.54 Sonnet Software, North Syracuse, NY, 2009.
88. J. Meng, S. Koziel, J.W. Bandler, M.H. Bakr, and Q.S. Cheng, Tuning space mapping: A novel technique for engineering design optimization, IEEE MTT-S Int Microwave Symp Dig, Atlanta, GA, June 2008, pp. 991–994.
89. S. Koziel, J. Meng, J.W. Bandler, M.H. Bakr, and Q.S. Cheng, Accelerated microwave design optimization with tuning space mapping, IEEE Trans Microwave Theory Tech 57 (2009), 383–394.
90. J.C. Rautio, EM-component-based design of planar circuits, IEEE Microwave Mag 8 (2007), 79–90.
91. Q.S. Cheng, J.W. Bandler, and S. Koziel, Tuning space mapping optimization exploiting embedded surrogate elements, IEEE MTT-S Int Microwave Symp Dig, Boston, MA, June 2009.
92. S. Ogurtsov and S. Koziel, Rapid surrogate-based optimization of UWB planar antennas, to appear, Eur Conf Antennas Propag 2010.
93. B. Beachkofski and R. Grandhi, Improved distributed hypercube sampling, American Institute of Aeronautics and Astronautics, paper AIAA 2002–1274, 2002.

BIOGRAPHIES

Qingsha S. Cheng was born in China. He received the B.Eng. and M.Eng. from Chongqing University, China, in 1995 and 1998, respectively. He received his Ph.D. at McMaster University, Canada, in 2004. In 1998, he joined the Department of Computer Science and Technology, Peking University, China. In 1999, he joined the Department of Electrical and Computer Engineering, McMaster University. Currently, he is a Research Associate in the Department of Electrical and Computer Engineering, McMaster University. His research interests are simulator-based tuning, surrogate modeling, computer-aided design, modeling of microwave circuits, software design technology, and methodologies for microwave CAD.

John W. Bandler studied at Imperial College and received the B.Sc.(Eng.), Ph.D., and D.Sc.(Eng.) degrees from the University of London, England, in 1963, 1967, and 1976, respectively. He joined McMaster University, Canada, in 1969. He is now a Professor Emeritus. He was President of Optimization

Systems Associates Inc., which he founded in 1983, until November 20, 1997, the date of acquisition by Hewlett-Packard Company. He is President of Bandler Corporation, which he founded in 1997. He is a Fellow of several societies, including the Royal Society of Canada. In 2004, he received the IEEE MTT-S Microwave Application Award.

Slawomir Koziel received the M.Sc. and Ph.D. degrees in electronic engineering from Gdansk University of Technology, Poland, in 1995 and 2000, respectively. He also received the M.Sc. degrees in theoretical physics and in mathematics, in 2000 and 2002, respectively, as well as the Ph.D. degree in mathematics in 2003, from the University of Gdansk, Poland. He is currently an Associate Professor with the School of Science and Engineering, Reykjavik University, Iceland. His research interests include CAD and modeling of microwave circuits, simulation-driven design, surrogate-based optimization, space mapping, circuit theory, analog signal processing, evolutionary computation, and numerical analysis.

Mohamed H. Bakr received the B.Sc. and M.Sc. degrees in Electronics and Communications Engineering and Engineering Mathematics from Cairo University, Egypt, in 1992 and 1996, respectively, with distinction (honors). He earned the Ph.D. degree in 2000 from McMaster University, followed by a year as NSERC Post Doctoral Fellow with the Computational Electromagnetics Research Laboratory, University of Victoria, Canada. He is currently an associate professor at McMaster University. His research areas of interest include computer-aided design and modeling of microwave and photonic circuits, and bioelectromagnetism. He is a principal contributor to the theories of electromagnetic adjoint sensitivities and space mapping optimization.

Stanislav Ogurtsov received the degree of physicist from Novosibirsk State University, Novosibirsk, Russia, in 1993, and the Ph.D. degree in electrical engineering from Arizona State University, Tempe, in 2007. He is currently a postdoctoral researcher at the Electromagnetic Optimization and Modeling Center, Reykjavik University, Iceland. His research interests include simulation-driven computer-aided design of RF, microwave, and millimeter-wave circuits, ultrawideband antennas, computational electromagnetics, modeling of high-speed digital circuits, and material characterization.